Nanoscale

PAPER

View Article Online
View Journal | View Issue

Cite this: *Nanoscale*, 2015, **7**, 2489

Torsional behaviors of polymer-infiltrated carbon nanotube yarn muscles studied with atomic force microscopy†

Cheong Hoon Kwon,[a] Kyoung-Yong Chun,[a] Shi Hyeong Kim,[a] Jae-Hyeok Lee,[b] Jae-Ho Kim,[b] Márcio D. Lima,[c] Ray H. Baughman[c] and Seon Jeong Kim*[a]

Received 7th September 2014,
Accepted 7th December 2014

DOI: 10.1039/c4nr05184j

www.rsc.org/nanoscale

Torsional behaviors of polymer-infiltrated carbon nanotube (CNT) yarn muscles have been investigated in relation to molecular architecture by using atomic force microscopy (AFM). Two polymers with different stiffnesses, polystyrene (PS) and poly(styrene-*b*-isoprene-*b*-styrene) (SIS), were uniformly infiltrated into CNT yarns for electrothermal torsional actuation. The torsional behaviors of hybrid yarn muscles are completely explained by the volume change of each polymer, based on the height and full width at half maximum profiles from the AFM morphological images. The volume expansion of the PS yarn muscle (1.7 nm of vertical change and 22 nm of horizontal change) is much larger than that of the SIS yarn muscle (0.3 nm and 11 nm change in vertical and horizontal directions) at 80 °C, normalized by their values at 25 °C. We demonstrate that their maximum rotations are consequently 29.7 deg mm^{-1} for the PS-infiltrated CNT yarn muscle (relatively larger rotation) and 14.4 deg mm^{-1} for the SIS-infiltrated CNT yarn muscle (smaller rotation) at 0.75 V m^{-1}. These hybrid yarn muscles could be applied in resonant controllers or damping magnetoelectric sensors.

Introduction

Carbon nanotube (CNT) yarn muscles have been recently introduced as torsional and tensile actuators, such as electrochemically operated torsional and rotational motors in the electrolyte,[1] and electrically, chemically, and photonically powered hybrid CNT yarn muscles.[2] These CNT-based yarns have been considered to be good torsional and tensile actuators with fast, high-force, large-stroke tensile and torsional behaviors. CNT-based yarn applications are regularly studied, and polymer yarns have also been recently introduced with powerful, high-stress and high-strength properties.[3] Their thermal actuations are largely driven by volume change (expansion or contraction) of the guest materials.[2]

So far, the torsional behaviors resulting from polymers with different moduli and stiffnesses have not been explored. In this study, two polymers, polystyrene (PS) and poly(styrene-*b*-isoprene-*b*-styrene) (SIS), were used as actuation guest materials. PS includes only hard segment PS blocks, but SIS consists of two hard PS end blocks and one soft, elastomeric polyisoprene mid-block. These two polymers induce specific volume change due to the morphological variations induced by phase transitions with increasing temperature. As a result, each polymer independently generates a quite different actuation degree and different behavior. In general, the degree of polymer volume change with temperature variation is measured using a melting point apparatus. Here, we suggest a simple and novel method using atomic force microscopy (AFM) as an alternative to identify the volume change associated with phase transitions and thermal expansion.

Diverse characterization results by AFM have been actively reported for CNT,[4,5] nanofibers/nanowires,[6–8] various polymers,[9–12] and biological systems,[13–15] in the past few decades. It is known that height expansion as measured by AFM is directly proportional to the volume expansion, based on the surface morphology of the polymers.[16–18] Furthermore, the percentage of volume expansion is determined from the minimum and maximum heights.[17] Therefore, understanding of the morphological change according to the phase transition of polymer is not only important for obtaining 'height' infor-

[a]*Center for Bio-Artificial Muscle and Department of Biomedical Engineering, Hanyang University, Seoul, 133-791, Korea. E-mail: sjk@hanyang.ac.kr*
[b]*Department of Molecular Science and Technology, Ajou University, Suwon, 443-749, Korea*
[c]*The Alan G. MacDiarmid NanoTech Institute, University of Texas at Dallas, Richardson, TX 75083, USA*

†Electronic supplementary information (ESI) available: Rotation speed results with increasing voltage for the hybrid yarn muscles, AFM topographical images, dynamic mechanical analyzer results (with storage modulus, loss modulus, and tangent δ), and AFM surface morphologies of the polymer-infiltrated CNT torsional yarn muscles. See DOI: 10.1039/c4nr05184j

mation from AFM analysis but also to determine the volume change with increasing or decreasing temperature. The surface morphology of polymer as obtained by AFM measurement at different temperatures directly provides the height information. The final torsional actuation was commonly caused by volume change of the polymer sample, which is investigated by height change of the AFM surface morphological images. In addition, their mechanical properties were estimated by force–distance curve, which is widely used for the determination of mechanical properties by measuring the interaction of the tip and sample. Estimation of Young's modulus from the force–distance curves also gives the stiffness information for the material.[19–21]

We demonstrate that the torsional behaviors of polymer-infiltrated CNT torsional yarn muscles are affected by different surface morphologies due to phase transitions with increasing and decreasing temperatures by AFM analysis. Consequently, the largest torsion is correlated with the highest volume expansion and the highest modulus of the polymer. The equilibrium state, dampening, response time, and period are also investigated, along with the discussion of Young's modulus and stiffness.

Experimental section

Materials

Commercial polystyrene (PS) with a melting point of 86–91 °C and poly(styrene-*b*-isoprene-*b*-styrene) (SIS) containing 22 wt% styrene were obtained from Sigma-Aldrich. Commercially purchased PS and SIS polymers were dissolved in toluene in various ratios. 10 wt% of each PS and SIS was dissolved in toluene.

Fabrication of polymer-infiltrated CNT yarn muscles

The yarns used in this work were drawn from ~400 μm high MWNT forests during the symmetric insertion of twist. A sheet of MWNTs was drawn from a MWNT forest. The MWNTs had an outer diameter of ~12 nm, contained ~9 walls, and formed large bundles.[32] The polymer-infiltrated CNT yarn muscles were fabricated with a two-end-tethered, bottom-half-infiltrated heterochiral yarn configuration. The twisting insertion was ~14 000 turns per meter. The yarn muscle for actuation was 4 cm long, with an average diameter of 24 μm, and it was composed of an inner structure showing a dual Archimedean scroll. Bare MWNT yarn was twisted into S-type by a motor. Then, the S-yarn was untwisted, and re-twisted into Z-type by a motor attached at one end in the other direction. The polymer-infiltrated CNT yarn muscles were fabricated using a simple infiltration method. After twisting the yarn, half of the segment was immersed in a polymer solution (PS or SIS) for 24 h at 25 °C, and then cured completely for 24 h. Hence, the heterochiral twist-spun yarn muscle was composed of a non-infiltrated CNT segment half and a polymer-infiltrated segment half having opposite chiralities with equal lengths (2 cm long). The paddle was placed at the interconnection (indicated in yellow, in Fig. 1A). The amount of guests (PS or SIS) contained in the yarn (2 cm long) was independently

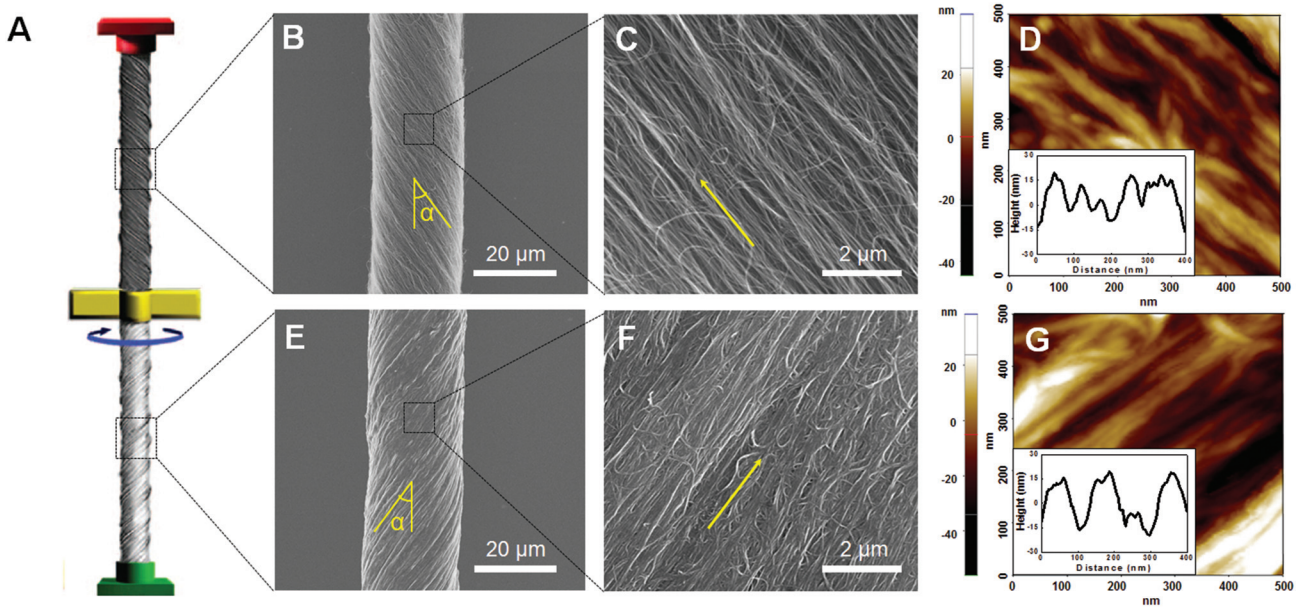

Fig. 1 Polymer-infiltrated CNT torsional yarn muscles. (A) Scheme of the biscrolled CNT yarn structure, a two-end-tethered, bottom-half-infiltrated polymer heterochiral yarn. (B and C) SEM images at low and high magnification of a torsional yarn actuator composed of bare CNT, (S type yarn, 23.0 μm diameter). (E and F) Polymer (PS)-infiltrated CNT torsional actuator (Z type yarn, 24.3 μm diameter), twisting insertion is 14 000 turns per meter and yarn bias angle, α, is 35°. Yellow arrows indicate the alignment directions of each segment. (D and G) AFM surface morphologies for a 500-nm square grid of guest-free CNT torsional yarn segment and polymer-infiltrated CNT torsional yarn segment. Inset: height profiles obtained by the surface morphology characterizations. (Average height/FWHM values were 27 nm/40 nm for PS, and 33 nm/53 nm for SIS, respectively.)

measured for each infiltrated segment. The guest mass was measured before and after guest infiltration using a microbalance to obtain the weight percentage of the guest in the yarn. The total weight of each yarn actuator containing PS or SIS was measured first, and the weight of the MWNT yarn without guest in the yarn was secondly measured. The percentage of yarn guest was finally calculated by subtracting the weight of MWNT yarn from the total weight of the yarn torsional actuator. The amount of PS contained in the yarn was 41 ± 2.5 μg (88 ± 0.5 wt%), and the amount of SIS in the yarn was 32 ± 2.2 μg (85 ± 0.8 wt%). The weight percentage of polymer in the yarn was determined based on three yarn samples. Accordingly, we confirmed that the amount of PS or SIS infiltrated in each yarn was similar.

Characterization

The surface morphologies and height profiles of the polymer-infiltrated CNT yarn were obtained using scanning electron microscopy (Hitachi S4700, Japan) and atomic force microscopy (AFM, Park Systems XE-100, South Korea). Electrically powered actuation was measured using a thermal mechanical analyzer (TMA, SEIKO TMA/SS7100), and each clamped yarn end was connected to a platinum wire using silver paste and then contacted to the voltage source-meter (Keithley 2635) after drying of the silver paste. A constant tensile stress of 0.35 MPa was applied by the TMA and the sample was excited by a 0.5 Hz square wave voltage using a 50% duty cycle. The tensile actuation was monitored using the TMA. The rotation angle (degree mm^{-1}) was precisely measured using a high speed imaging camera with a high resolution (2000 frame s^{-1}, Phantom Miro eX2). The loss tangent was obtained using a dynamic mechanical analyzer (DMA, Perkin Elmer instrument, $\tan\delta = E''/E'$) from the storage modulus (E') and loss modulus (E''). The yarn tested by DMA was 5 mm in length. The yarn samples were cooled to −70 °C and measured during heating from −70 to 90 °C with a 5 °C min^{-1} rate. An oscillation of 1 Hz was continuously applied. The hybrid yarn was vertically mounted in the DMA and operated in a dry nitrogen environment, purged at 50 ml min^{-1}.

Results and discussion

Polymer-infiltrated CNT torsional yarn muscles

The torsional actuation of CNT torsional yarn muscles containing different polymers was measured. The configuration of the polymer–CNT yarn under a tensile load, tethered at both ends, is presented in Fig. 1A. The biscrolled polymer–CNT torsional yarn muscle was composed of an S type (right-hand inserted twist) guest-free CNT yarn half and an opposite half of Z type (left-hand inserted twist) polymer guest-infiltrated CNT yarn. The paddle was attached at the mid-point between the S and Z yarn segments of the whole yarn muscle.

The heterochiral yarn muscle was actuated along only one half of the yarn segment. In other words, since the guest in the guest-filled Z yarn segment does not completely melt during guest heating, the unmelted guest acts as an internal return spring that allows the paddle to return to the starting rotation angle when the torsional actuation is reversed by guest cooling.[22] The scanning electron microscopy (SEM) images in Fig. 1B and E show the surface images of the non-infiltrated S segment and the infiltrated Z segment having the same 35° bias angle, which is the inclination angle of the CNTs with respect to the yarn direction. Their enlarged SEM yarn surface images are shown in Fig. 1C and F, respectively. Both the guest-free-CNT and polymer–CNT segments were symmetrically twist-spun from multi-walled carbon nanotubes (MWNT) consisting of helices with only one chirality, and their structures were well-oriented with a constant bias angle. Especially, the polymer guest was easily infiltrated into the CNT torsional yarn muscle, and the surface morphology of the polymer–CNT segment (Fig. 1F) was much denser and polymer-solution-covered overall, unlike the surface morphology of the guest-free-CNT segment (Fig. 1C). Additionally, representative AFM surface topographic images are shown in Fig. 1D and G as examples of guest-free and polymer guest-filled yarn composite segments in a square with the length of 500 nm.

Torsional actuation behaviors

The torsional actuations of the two-end tethered yarns are shown in Fig. 2. As the voltage was increased from 0 to

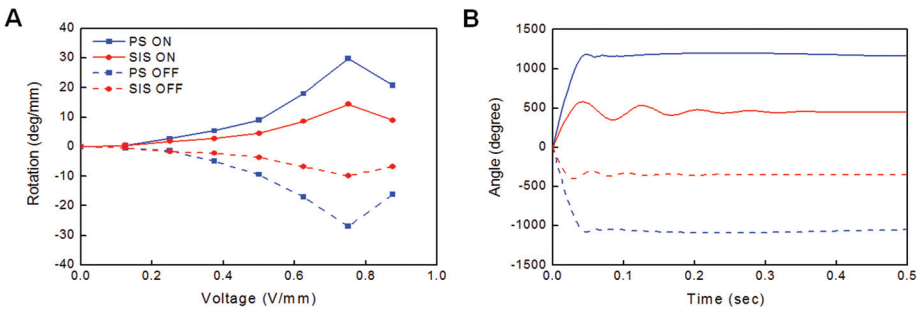

Fig. 2 Torsional behaviors of the polymer-infiltrated CNT yarns. The blue symbols and blue lines correspond to PS-infiltrated CNT, and the red symbols and red lines correspond to SIS-infiltrated CNT. (A) Thermal torsional actuation for the polymer-infiltrated CNT yarns versus the applied voltage for a 0.5 Hz square-wave-voltage using a 50% duty cycle, when the drive voltage is turned on (solid line) and turned off (dotted line). (B) Step response of the under-damped process with torsional rotation angle versus time for the PS-infiltrated CNT yarn (blue line) and SIS-infiltrated CNT yarn (red line), when the drive voltage is turned on (solid line) and turned off (dotted line).

0.88 V mm^{-1}, the torsional rotation also increased for the hybrid yarns until the glass transition temperature (T_g) was reached, and then, the torsional rotation gradually reduced at temperatures above T_g. The chemical structure changes and molecular mobilities of materials are affected by the molecular weight and the stiffness of the molecular chain; intermolecular attractive and repulsive forces are largely dependent on T_g. The voltage range showing the maximum torsional actuation was 0.7–0.8 V mm^{-1} for the two different hybrid yarn muscles. The two polymers have a similar T_g point for PS[23] and SIS[24] near 90 °C (in addition, SIS has another T_g point near −40 °C). When they are heated, the PS domains soften and SIS becomes processable as a thermoplastic. When solidified, SIS exhibits good elastomeric properties as the PS domains reform and strength returns.

As shown in Fig. 2A, actuation of the PS-infiltrated CNT torsional yarn generates a larger rotation compared with the SIS-infiltrated CNT yarn. Their maximum rotations, 29.7 deg mm^{-1} for the PS-infiltrated CNT yarn and 14.4 deg mm^{-1} for the SIS-infiltrated CNT yarn, were obtained at 0.75 V m^{-1}. Their rotational speeds were also measured as a function of the voltage, as shown in Fig. S1.† The maximum rotational speeds were 781.6 and 279.6 rpm for the PS and SIS-infiltrated CNT yarn muscles at 0.75 V m^{-1}, respectively. The region showing the maximum torsional rotation is closely related to the T_g of the two polymers. Around the T_g, the PS-infiltrated CNT torsional yarn shows rapid rotation according to the high volume expansion degree of PS compared to SIS-infiltrated CNT yarn. At temperatures above T_g, the torsional rotation started to decline, due to the deformational change of the polymer at higher temperatures than T_g.

Fig. 2B shows the dependence of torsional rotation on time during forward and reverse actuation at 0.75 V mm^{-1} with a 50% duty cycle. The two polymer-infiltrated CNT yarns exhibited oscillation in the forward and reverse actuation process. The maximum final rotational angle of the PS-infiltrated CNT torsional actuator (1188 degree) is twice as high as that of the SIS-infiltrated CNT yarn (576 degrees), and the settling time of the PS-infiltrated CNT yarn (~0.1 s) is shorter than that of the SIS-infiltrated CNT yarn (~0.4 s). The settling time for the polymer-infiltrated CNT torsional yarns is defined as the time required for the process output to reach and remain inside a band whose width is equal to ±1% of the total angle change. From the different torsional behaviors of the hybrid yarns, it is found that the PS-infiltrated CNT yarn muscle shows faster settling, and a shorter period (~0.02 s) than the SIS yarn (~0.08 s).

The period of oscillation for each polymer-infiltrated CNT yarn is the time between two successive peaks or two successive valleys of the response (Fig. 2B). The torsional muscles show both under-damped responses (0 < damping ratio, $\zeta < 1$), which show over-shoot of the equilibrium position (37.9% for the PS-infiltrated CNT yarn, and 77.2% for the SIS-infiltrated CNT yarn) and gradually oscillate with decreasing amplitude to reach a stable equilibrium. The damping ratios were 0.36 and 0.15 for the PS and SIS actuators, respectively, obtained using the ratio of the rotation angle peak heights.[25] The PS yarn muscle, which shows a high damping ratio, is considered to operate with relatively stable torsional behavior. In addition, the torsional stiffness of the PS yarn (1.5×10^{11} N m) was greater than that of the SIS yarn (0.4×10^{11} N m). Their different torsional behaviors were investigated by volume expansion degree related to the phase transition in the next sections.

AFM characterization of phase transition and thermal expansion

Thermal expansion of the polymers induces an increase in the yarn volume, the contraction of the yarn length, and untwisting of the yarn with torsional actuation. An AFM system was employed for the verification of the phase transitions of polymer guests. AFM characterizations were conducted in non-contact mode with the intensity corresponding to height. The cantilevers (Arrow NCR-50, NanoWorld Corp., Switzerland) were 160 μm long with a resonant frequency of 280–300 kHz and a force constant of 42 N m^{-1}. The scan speed was 1 line of 256 pixels per second. The morphological 3D AFM images for investigating the phase transitions of the PS and SIS polymers, as the temperature was increased from 25 °C to 150 °C, are shown in Fig. 3 and 4. To explain the degree of the phase change, we used the average height profiles and full width at half maximum (FWHM) profiles from the morphology analysis. These two factors are closely related to the vertical and horizontal volume changes as a function of temperature.

A notable phase change of the PS polymer in the yarn was clearly observed in Fig. 3, and the average heights and FWHMs are shown in Fig. 3E–H. At 25 °C, the morphology of the PS was relatively flatter (Fig. 3A–D) with an average height of 0.44 nm and a FWHM of 8.55 nm. At 40 °C, the morphology was not significantly changed compared to 25 °C, with an average height of 0.70 nm and a FWHM of 10.07 nm. However, near the T_g region at 80 °C, crater-like holes evidently appeared in the surface morphology, and a volume change (Fig. 3C and G) was reflected in the 2.17 nm average height and 30.55 nm FWHM. When heated to 150 °C, the polymer surface underwent deformational change as shown in Fig. 3D. At this temperature, the average height and FWHM were 3.59 nm and 116.12 nm, respectively. Additionally, the surface roughness increased to 0.14, 0.21, 0.48 and 1.17 for 25, 40, 80 and 150 °C, respectively. Rough surfaces usually wear more quickly and have higher friction coefficients than smooth surfaces.[26] In other words, at temperatures which generate polymer degradation, a larger roughness indicates a proportionally larger phase transition, resulting in higher torsional actuation. Likewise, the phase transition of SIS polymer was studied in the same way, as shown in Fig. 4. The AFM image uniformly exhibited lamellae-type structures resulting from the phase behavior of the SIS block copolymer. Compared to the PS polymer, the surface morphological changes (Fig. 4A–D) and the related average height and FWHM changes (Fig. 4E–H) of SIS were relatively small.

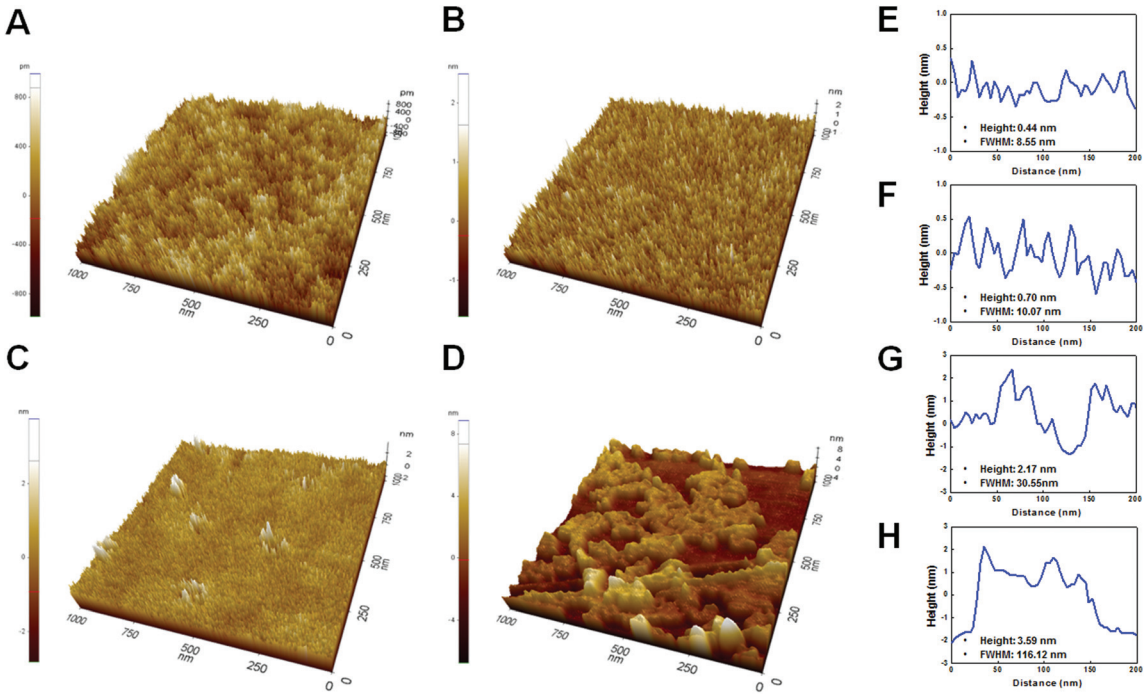

Fig. 3 PS polymer film (without CNT) morphology characterization by AFM measurement as a function of temperature. (A and E) High-resolution 3D AFM image (for a 1 μm square grid) and line profile from the image (A) at 25 °C. (B and F) AFM image and line profile from the image (B) at 40 °C. (C and G) AFM image and line profile from the image (D) at 80 °C. (D and H) AFM image and line profile from the AFM image (D) at 150 °C.

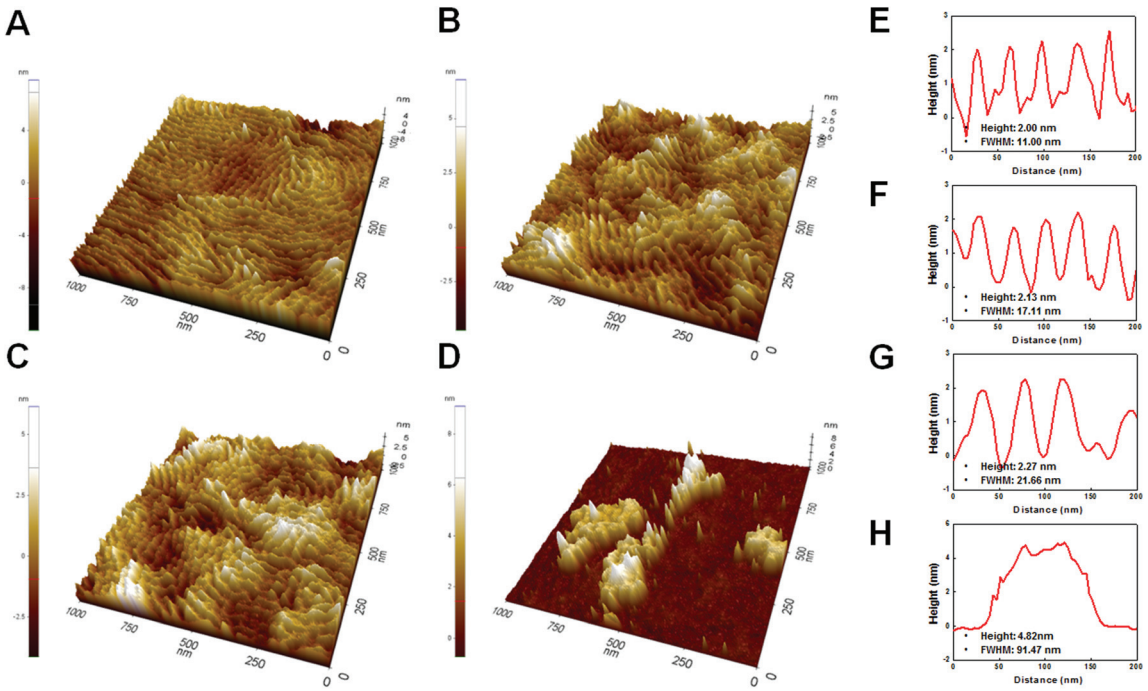

Fig. 4 SIS polymer film (without CNT) morphology characterization by AFM measurement as a function of temperature. (A and E) High-resolution AFM 3D image (for 1-μm square grid) and line profile from the image (A) at 25 °C. (B and F) AFM image and line profile from the image (B) at 40 °C. (C and G) AFM image and line profile from the image (C) at 80 °C. (D and H) AFM image and line profile from the AFM image (D) at 150 °C.

The height profile changed from 2.00 nm to 4.82 nm, and the FWHM changed from 11.00 nm to 91.47 nm. The roughness of the SIS polymer changed from 0.62 at 25 °C to 1.88 at 150 °C (0.65 at 40 °C and 0.69 at 80 °C). 2D AFM topographic images of PS and SIS are also shown in Fig. S2 and S3,† respectively.

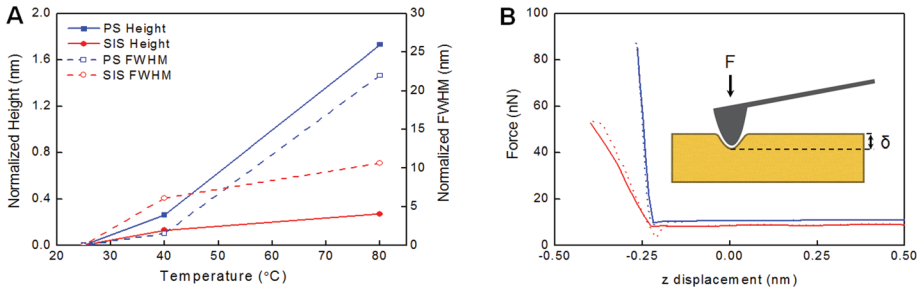

Fig. 5 Normalized height and FWHM profiles for PS and SIS, and the *F–D* curve of the PS-infiltrated CNT yarn and the SIS-infiltrated CNT yarn determined using AFM measurement. (A) Evaluation of the normalized height (left axis, blue closed symbol and solid line for PS, and red closed symbol and solid line for SIS) from the surface morphology. The normalized FWHM (right axis, blue open symbol and dashed line for PS, and red open symbol and dashed line for SIS) determined using AFM as a function of temperature, from 25 °C to 80 °C (near the T_g of the polymers). (B) Force and distance curves of the PS-infiltrated CNT (blue) and SIS-infiltrated CNT (red) torsional yarn actuators using an AFM tip (NSC-36 contact cantilever) with a spring constant of 0.6 N m^{-1}. The tracing (solid line) and retracing (dotted line) speed of the cantilever was 100 nm s^{-1}. Inset: scheme of the AFM tip, δ is the indentation depth, and F is the applied force.

The height and FWHM values of the AFM morphologies were normalized by their values for the two polymers at 25 °C. The normalized height and FWHM of PS and SIS were plotted at three temperature conditions (25, 40 and 80 °C) in Fig. 5A. Near the 80 °C temperature region, the normalized height of the PS yarn increased dramatically to 1.7 nm, compared to the SIS yarn (0.3 nm), and the normalized FWHM of the PS yarn also increased to 22.0 nm, while that of the SIS yarn was 10.7 nm. Although the volume expansion was maximized at 150 °C according to the height and FWHM profiles, the maximum torsional degree was not obtained at that condition due to the polymer degradation. From the clear difference in these two significant factors, it was found that the volume expansion of the PS yarn (1.7 nm of vertical change and 22 nm of horizontal change with normalization by their values at 25 °C) is much larger than that of SIS yarn (0.3 nm and 11 nm changes in the vertical and horizontal directions, with normalization in the same way) from the AFM morphological images at a temperature of 80 °C.

Torsional behaviors from Young's modulus and stiffness

The elastic behavior and the stiffness of a material are typically measured by its deformation response to an applied force. Especially, stiffness has been investigated using Young's modulus, obtained by AFM.[27,28] To estimate Young's modulus, we used force and distance (F/D) curves, which are another major application of AFM and measuring tip–sample interactions, using a NSC-36 contact cantilever (MikroMash Inc., USA) with a resonance frequency ≈65 kHz, radius of curvature ≈10 nm, and length of 130 ± 5 μm. This method extends the elastic continuum contact theories to plastic deformations and permits calculation of the stiffness in the plastic regime of deformation. We measured the F/D curves of the PS and SIS-infiltrated CNT torsional yarn actuators at 25 °C as shown in Fig. 5B. The maximum loading forces applied were 85 ± 1.3 nN and 52 ± 5.8 nN for PS and SIS on average, respectively. Furthermore, the slope of the PS-infiltrated CNT torsional actuator was sharper than that of the SIS-infiltrated CNT torsional actuator. This means that the PS-infiltrated CNT yarn is mechanically stiffer than the SIS-infiltrated CNT yarn, as well.

To estimate Young's modulus, we directly applied Hertzian theory for viscoelastic materials[29] to the maximum loading forces (Fig. 5B) from the AFM indentation test. This procedure shows the stiffness differences along the indentation path, and gives information about the surface topography and the interior mechanical properties of the sample. Young's modulus for the polymer-infiltrated CNT yarn was estimated according to the following equation for a parabolic tip geometry[29]:

$$F = \frac{4\sqrt{R_c}}{3}\frac{E}{1-\nu}\delta^{3/2}$$

where R_c, δ, and ν represent the radius of tip curvature, indentation depth, and Poisson's ratio of the sample, respectively. Poisson's ratio (ν) is equal to 1/2 for an incompressible material.[30] F is the maximum load, and E is the calculated Young's modulus. When there are changes in the Force-Z displacement, the cantilever will deflect to the direction opposite that at which the tip contacts the sample. Based on their Young's moduli, the PS-infiltrated CNT torsional yarn muscle was stiffer (116 ± 2.7 kPa) than the SIS-infiltrated CNT torsional yarn muscle (67 ± 8.6 kPa). The stiffness of the polymer-infiltrated CNT yarn muscle, which was estimated by Young's modulus, was related to the torsional actuation degree and torsional behaviors. The torsional degree of the stiff polymer (PS)-infiltrated CNT yarn was larger than that of the relatively soft polymer (SIS)-infiltrated CNT yarn, and the stiff-material-based CNT yarn exhibited faster settling and a shorter period than the soft-material-based CNT yarn.

The Young's moduli of the polymers determined through AFM measurements were also in agreement with the values from dynamic mechanical analyzer (DMA) measurements. DMA provides information related to the damping properties of the polymer-infiltrated CNT yarn actuators.[22] First of all, the temperature dependence of the loss tangent (tan $\delta = E''/E'$)

determined from the storage modulus (G', Fig. S4A†) and loss modulus (G'', Fig. S4B†) were determined at a frequency of 1 Hz for the PS and SIS-infiltrated CNT torsional yarn muscles in Fig. S4C.† The ratio of the loss to the storage is often called damping, which is a measure of the energy dissipation of a material. The PS-infiltrated CNT yarn torsional actuator was shown to exhibit rapid rotation according to the high intensity of tan δ as compared to the SIS-infiltrated CNT yarn actuator. This means that the PS-infiltrated CNT yarn torsional actuator shows a relatively large damping compared to the SIS-infiltrated CNT yarn actuator. In addition, PS shows one peak at the glass transition while SIS actually exhibits two independent peaks of loss factor (tan δ) corresponding to the glass transitions of the polyisoprene and polystyrene segments. However, only one peak each for PS and SIS was shown above 0 °C. The PS and SIS peaks associated with the damping properties depended on the temperature from 0 to 150 °C. With increasing amount of the softening block (polyisoprene) in the polymer, the main tan δ peak shifted to higher temperatures.[31] As shown in Fig. S4C, the † tan δ peak of SIS is shifted to higher temperature, indicating that SIS containing an isoprene mid-block is mechanically softer than PS polymer.

The surface morphologies and volume changes of our polymer-infiltrated CNT yarn muscles were also verified in Fig. S5.† Compared to the guest-free CNT yarn (Height: 27.12 nm, FWHM: 39.62 nm) (Fig. S5A and D†), the PS and SIS-infiltrated CNT yarns exhibited greater height and FWHM values at 25 °C. Especially, horizontal volume expansion with obvious FWHM change (78.68 nm) was verified for the the PS-infiltrated CNT yarn muscle (Fig. S5B and E†), as compared to the value of the SIS-infiltrated CNT yarn muscle (52.98 nm, in Fig. S5C and F†).

Conclusions

We demonstrated that the thermal torsional actuation of the polymer-infiltrated CNT yarn muscles was driven by volume changes associated with phase transitions of the guest materials. Using AFM measurements, the torsional behaviors of the hybrid yarns were investigated along with their physical properties such as Young's moduli and stiffnesses. The torsional behaviors of the PS and SIS-infiltrated CNT yarn muscles were simply described with the surface morphologies of each polymer by AFM analysis. Polymer-infiltrated CNT torsional yarn muscles could potentially be applied in resonant controllers or damping magnetoelectric sensors, in which the signal of magnetic sensors based on resonant cantilevers comprised of elastically coupled piezoelectric and magnetostrictive materials increases as the damping decreases.

Acknowledgements

Supported by the Creative Research Initiative Center for Bio-Artificial Muscle of the Ministry of Education, Science and Technology (MEST) and the MEST-US Air Force Cooperation Program (Grant No. 2012-00074) in Korea; Air Force Grant AOARD-10-4067, Air Force Office of Scientific Research grant FA9550-12-1-0211, and Robert A. Welch Foundation grant AT-0029 in the USA; and the Australian Research Council through the Centre of Excellence and Fellowship programs.

Notes and references

1 J. Foroughi, G. M. Spinks, G. G. Wallace, J. Oh, M. E. Kozlov, S. Fang, T. Mirfakhrai, J. D. W. Madden, M. K. Shin, S. J. Kim and R. H. Baughman, *Science*, 2011, **334**, 494.
2 M. D. Lima, N. Li, M. J. Andrade, S. Fang, J. Oh, G. M. Spinks, M. E. Kozlov, C. S. Haines, D. Suh, J. Foroughi, S. J. Kim, Y. Chen, T. Ware, M. K. Shin, L. D. Machado, A. F. Fonseca, J. D. W. Madden, W. E. Voit, D. S. Galvão and R. H. Baughman, *Science*, 2012, **338**, 928.
3 C. S. Haines, M. D. Lima, N. Li, G. M. Spinks, J. Foroughi, J. D. W. Madden, S. H. Kim, S. Fang, M. J. Andrade, F. Göktepe, Ö. Göktepe, S. M. Mirvakili, S. Naficy, X. Lepró, J. Oh, M. E. Kozlov, S. J. Kim, X. Xu, B. J. Swedlove, G. G. Wallace and R. H. Baughman, *Science*, 2014, **343**, 868.
4 J. Liu, M. J. Casavant, M. Cox, D. A. Walters, P. Boul, W. Lu, A. J. Rimberg, K. A. Smith, D. T. Colbert and R. E. Smalley, *Chem. Phys. Lett.*, 1999, **303**, 125.
5 J. H. Kim, M. -J. Song, C. J. Lee, J.-H. Lee, J. -H. Kim and N. K. Min, *Carbon*, 2013, **52**, 398.
6 M. K. Shin, S. I. Kim, S. J. Kim, S.-K. Kim and H. Lee, *Appl. Phys. Lett.*, 2006, **88**, 193901.
7 A. Noy, A. E. Miller, J. E. Klare, B. L. Weeks, B. W. Woods and J. J. DeYoreo, Fabrication of Luminescent Nanostructures and Polymer Nanowires Using Dip-Pen Nanolithography, *Nano Lett.*, 2002, **2**, 109.
8 B. W. Maynor, S. F. Filocamo, M. W. Grinstaff and J. Liu, *J. Am. Chem. Soc.*, 2002, **124**, 522.
9 A. Star, J. F. Stoddart, D. Steuerman, M. Diehl, A. Boukai, E. W. Wong, X. Yang, S.-W. Chung, H. Choi and J. R. Heath, *Angew. Chem., Int. Ed.*, 2001, **40**, 1721.
10 J. Couet, J. D. J. S. Samuel, A. Kopyshev, S. Santer and M. Biesalski, *Angew. Chem., Int. Ed.*, 2005, **44**, 3297.
11 R. S. McLean and B. B. Sauer, *Macromolecules*, 1997, **30**, 8314.
12 Y. Chen and J. T. Koberstein, *Langmuir*, 2008, **24**, 10488.
13 M. Tsoi, T. T. Do, V. Tang, J. A. Aguilera, C. C. Perry and J. R. Milligan, *Biophys. Chem.*, 2010, **147**, 104.
14 T. G. Kuznetsova, M. N. Starodubtseva, N. I. Yegorenkov, S. A. Chizhik and R. I. Zhdanov, *Micron*, 2007, **38**, 824.
15 H. Haga, S. Sasaki, K. Kawabata, E. Ito, T. Ushiki and T. Sambongi, *Ultramicroscopy*, 2000, **82**, 253.
16 R. B. Lewis, A. Timmons, R. E. Mar and J. R. Dahn, *J. Electrochem. Soc.*, 2007, **154**, A213.
17 Y. Tian, A. Timmons and J. R. Dahn, *J. Electrochem. Soc.*, 2009, **156**, A187.

18 E. Smela and N. Gadegaard, *J. Phys. Chem. B*, 2001, **105**, 9395.
19 M. Motomatsu, W. Mizutanit and H. Tokumoto, *Polymer*, 1997, **38**, 1779.
20 B. Cappella, S. K. Kaliappan and H. Sturm, *Macromolecules*, 2005, **38**, 1874.
21 S. Tripathy and E. J. Berger, *J. Biomech. Eng.*, 2009, **131**, 094507.
22 K.-Y. Chun, S. H. Kim, M. K. Shin, C. H. Kwon, J. Park, Y. T. Kim, G. M. Spinks, R. H. Baughman and S. J. Kim, *Nat. Commun.*, 2014, **5**, 1.
23 S. Ghosh, D. Khastgir and A. K. Bhowmick, *J. Appl. Polym. Sci.*, 1998, **67**, 2015.
24 C. D. Han, J. Kim, J. K. Kim and S. G. Chu, *Macromolecules*, 1989, **22**, 3443.
25 C.-T Huang and C.-J. Chou, *Ind. Eng. Chem. Res.*, 1994, **33**, 174.
26 E. P. Degarmo, J. T. Black, R. A. Kohser and B. E. Klamecki, *Materials and Processes in Manufacturing*, John Wiley & Sons Inc., 9th edn, 2003, 223.
27 C. Roduit, S. Sekatski, G. Dietler, S. Catsicas, F. Lafont and S. Kasas, *Biophys. J.*, 2009, **97**, 674.
28 S. N. Magonov, V. Elings and M.-H. Whangbo, *Surf. Sci.*, 1997, **375**, L385.
29 H. Hertz, *J. Reine Angew. Math.*, 1882, **92**, 156.
30 K. Thongsak, R. Kunanuruksapong, A. Sirivat and W. Lerdwijitjarud, *Mater. Sci. Eng., A*, 2010, **527**, 2504.
31 C. Wu, G. Wu and C. Wu, *J. Appl. Polym. Sci.*, 2006, **102**, 4157.
32 M. Zhang, K. R. Atkinson and R. H. Baughman, *Science*, 2004, **306**, 1358.

